

The scalar Singlet-Triplet Dark Matter Model

O. Fischer^{*} and J.J. van der Bij[†]

*Physikalisches Institut, Albert-Ludwigs-Universität Freiburg -
Fakultät für Mathematik und Physik, D-79104 Freiburg, Germany*

Abstract

We consider a model for cold dark matter, which combines a real scalar singlet and a real scalar $SU(2)_L$ triplet field, both of which are residing in the odd representation of a global Z_2 symmetry. The parameter space of the model is constrained by the inferred dark matter abundance from the WMAP and Planck data, the most recent results from the direct dark matter search experiment LUX, the Z boson decay width from LEP-I and perturbativity of the coupling parameters. The phenomenology of the remaining parameter space is studied. We find that the model allows for DM masses near the electroweak scale and a variety of decay scenarios.

^{*} e-mail: oliver.fischer@physik.uni-freiburg.de

[†] e-mail: vdbij@uni-freiburg.de

I. INTRODUCTION

One of the most astounding revelations of the twentieth century for our understanding of the Universe was the discovery of non-baryonic dark matter [1, 2], which is about five times more abundant than baryonic matter. Up to now, dark matter is undetected in the laboratory. It also drives structure formation on large scales and determines galactic and extra-galactic dynamics. The interpretation of dark matter as representing a type of elementary particle, is the most studied and most successful. Since the standard model (SM) of particle physics does not provide a viable candidate for a dark matter particle, an extension of the SM is necessary. In general a Weakly Interacting Massive Particle (WIMP) is the preferred object, with masses between about ten and a few hundred GeV.

Aside from its precise nature, which will be difficult to establish, a new unbroken symmetry seems to be fundamental for dark matter particles. If the latter are charged under this symmetry they can be stable on cosmological time scales. Most of the popular dark matter models start with a motivation, which is not directly related to the dark matter problem, but nevertheless leads to a natural inclusion of suitable particle candidates.

Commonly supersymmetry is invoked as a principle, where then R-parity is taken as the conserved symmetry. In this case the lightest supersymmetric particle would be the dark matter candidate and a relation between supersymmetry and dark matter is claimed to exist. This argument is misleading. R-parity is an independent principle, introduced to avoid supersymmetric rapid proton decay. Since supersymmetry by itself does not imply R-parity, it is not supersymmetry that gives a natural dark matter candidate.

If simplicity is invoked as the main principle, scalar singlet fields [3–8] are preferred as the simplest candidate for dark matter.

The next simplest candidate for dark matter is given by a real scalar $SU(2)_L$ -triplet field, as presented and studied in Refs. [9–11]. This particle is a suitable dark matter candidate, because radiative corrections to its mass render the neutral component lighter than the charged ones.

Besides the precise nature of the dark matter particle it is a priori unclear whether the dark matter consists of one or more components. An interesting suggestion for a multi-component form of dark matter was made in [12]. It was argued that the dark matter should be part of a matter-parity odd representation of the unification group $SO(10)$, the

smallest being the **16**, which led to a combination of an inert doublet and a complex singlet. In the original motivation for this model, results from ref.[13, 14] were used. In ref.[13, 14] an argument was presented, that the fermions should come in exactly three generations of a **16**-spinor representation of $SO(10)$ [13, 14]. However it was found that the unification group should be $SU(5)$ and not $SO(10)$. When a matter parity is included in such a unification scenario, it is very likely that a larger number of fields reside in matter-parity odd representations, which implies a multicomponent dark matter scenario. In particular, when the **24**-representation of $SU(5)$ is considered, beyond the Standard Model fields, a real singlet plus a $SU(2)_L$ triplet field are found. Since no experiment has detected such fields up to now, it is straightforward to assume that they have odd matter-parity, and thus might yield viable dark matter candidates. Both fields couple to the Higgs boson, so that they scatter off terrestrial nuclei, which makes them sensitive to the null-results coming from direct detection experiments [15].

The combination of singlet and triplet dark matter fields will be studied in the following. Contrary to previous work in Ref. [16], we postulate *one* dark matter symmetry, which leads to interesting phenomenological implications.

This paper is structured in the following way: In the next section, we introduce the singlet-triplet Z_2 model as an extension of the SM, which includes one global Z_2 symmetry and a real scalar singlet and a real scalar $SU(2)_L$ triplet field to the matter content of the Theory. Including all the renormalizable terms in the Lagrangian leads to mass mixing of the singlet and triplet fields after spontaneous symmetry breaking. In section III we study the effect of the abundance constraint on the parameter space of the model by employing the numerical tool micrOMEGAs [17, 18]. This leads to three distinct scenarios, namely the singlet, the triplet and the mixed scenario, which will be discussed in separate subsections. Section IV contains our summary and the conclusions.

II. THE MODEL

The matter content of the SM is extended with two real scalar fields: a singlet Φ and a $SU(2)_L$ triplet. Both fields reside in the odd representation of an additional, global Z_2 symmetry, while the SM fields reside in the even representation.

The Lagrangian of the singlet-triplet Z_2 model reads:

$$\mathcal{L}_{Z_2} = \mathcal{L}_{\text{SM}} + \mathcal{L}_{\Phi} + \mathcal{L}_{\Psi} + \mathcal{L}_{\text{mix}}, \quad (1)$$

where \mathcal{L}_{SM} contains the usual SM fields and

$$\mathcal{L}_{\Phi} = \frac{1}{2} \partial_{\mu} \Phi \partial^{\mu} \Phi - \frac{1}{2} m_{\Phi}^2 \Phi^2 - \frac{\lambda_{\Phi}}{4!} \Phi^4 - \frac{\omega_{\Phi}}{4} \Phi^2 H^{\dagger} H, \quad (2)$$

$$\mathcal{L}_{\Psi} = \frac{1}{2} \mathcal{D}_{\mu} \Psi^{\dagger} \mathcal{D}^{\mu} \Psi - \frac{1}{2} m_{\Psi}^2 |\Psi|^2 - \frac{\lambda_{\Psi}}{24} |\Psi|^4 - \omega_{\Psi} |\Psi|^2 H^{\dagger} H, \quad (3)$$

$$\mathcal{L}_{\text{mix}} = \kappa H^{\dagger} \tau^i H \Psi_i \Phi + \kappa' \Phi^2 |\Psi|^2. \quad (4)$$

In the above equations, H is the SM Higgs doublet, $\lambda_{\Phi}, \lambda_{\Psi}, \omega_{\Phi}, \omega_{\Psi}$ and κ are dimensionless coupling constants, m_{Φ}, m_{Ψ} are the Lagrange masses of the singlet and triplet respectively. In the following, the coupling parameters $\lambda_{\Phi}, \lambda_{\Psi}, \kappa'$ will be neglected, since their contribution to the dark matter abundance was shown to be irrelevant [16].

The spontaneous breaking of the electroweak symmetry leads to a mixing of the neutral flavour eigenstates Φ, Ψ^0 through the first term in eq. (4). The mixed fields S_1 and S_2 are linear combinations of the interaction eigenstates, which can be expressed as

$$\begin{pmatrix} \Phi \\ \Psi^0 \end{pmatrix} = \begin{pmatrix} c_{\delta} & s_{\delta} \\ -s_{\delta} & c_{\delta} \end{pmatrix} \begin{pmatrix} S_1 \\ S_2 \end{pmatrix}, \quad (5)$$

where $s_{\delta} (c_{\delta})$ are the sine (cosine) of the mixing angle δ . For conformity, the charged triplet components are relabeled to $S^{\pm} \equiv \Psi^{\pm}$ and the mass $m_c \equiv m_{\Psi} + \Delta m$, where Δm is the loop-induced mass splitting due to the gauge couplings of the triplet field [11].

The physical masses of the fields S_1, S_2, S^{\pm} , or S -fields for brevity, are given by the eigenvalues of the mass matrix:

$$m_{\pm}^2 = \frac{1}{2} \left[m_{\Phi}^2 + m_{\Psi}^2 \pm \sqrt{(\Delta)^2 + \kappa^2 v^4} \right], \quad (6)$$

with $\Delta = m_{\Phi}^2 - m_{\Psi}^2$. We identify m_{-}, m_{+} with m_1, m_2 respectively. The mixing angle can be expressed in terms of the physical masses as

$$s_{\delta}^2 = \frac{1}{2} \left[1 - \sqrt{1 - \frac{\kappa^2 v^4}{(m_1^2 - m_2^2)^2}} \right]. \quad (7)$$

The mass splitting between m_1 and m_c can be defined via a mass-splitting parameter c , as

$$c \equiv \frac{m_c}{m_1}. \quad (8)$$

We have the following useful relations between parameters:

$$m_2^2 = m_1^2 \left[1 + \frac{c^2 - 1}{c_\delta^2} \right] \quad (9)$$

$$\kappa = 2 t_\delta (c^2 - 1) \frac{m_1^2}{v^2}. \quad (10)$$

Note that in the limit of δ going to zero, m_2 converges to m_c and κ to zero, as it should. It is convenient to define the mass splitting between S^\pm and S_2 , analogous to the definition in eq. (8), as

$$c_2 \equiv \frac{m_2}{m_1} = \frac{\sqrt{c^2 - s_\delta^2}}{c_\delta}. \quad (11)$$

The couplings ω_{ij} , defined via the terms HS_iS_j are given by

$$-\omega_{11} \equiv 4 s_\delta c_\delta \kappa - c_\delta^2 \omega_\Phi - s_\delta^2 \omega_\Psi, \quad (12)$$

$$-\omega_{12} \equiv -2 (s_\delta^2 - c_\delta^2) \kappa - s_\delta c_\delta (\omega_\Phi - \omega_\Psi), \quad (13)$$

$$-\omega_{22} \equiv -4 s_\delta c_\delta \kappa - s_\delta^2 \omega_\Phi - c_\delta^2 \omega_\Psi. \quad (14)$$

While ω_Φ, ω_Ψ are free parameters, κ is a function of the model parameters m_1, c, δ . In defining the Lagrange parameters ω_Φ, ω_Ψ as functions of the effective Higgs couplings ω_{11}, ω_{22} , the latter become the free parameters of the model. This choice of parameter set gives

$$-\omega_{12} = \frac{2\kappa}{c_\delta^2 - s_\delta^2} - \frac{s_\delta c_\delta \omega_{11}}{c_\delta^2 - s_\delta^2} - s_\delta c_\delta \omega_{22}, \quad (15)$$

$$-\omega_\Psi = \frac{4s_\delta c_\delta \kappa - c_\delta^2 \omega_{22} - s_\delta^2 \omega_{11}}{s_\delta^2 - c_\delta^2}. \quad (16)$$

The perturbativity of the theory is violated with $|\omega_{12}|, |\omega_\Psi| > 1$, which defines upper bounds for the model parameters c, δ :

$$c_{\max} = \sqrt{\frac{v^2}{t_\delta m_1^2} + 1}, \quad (17)$$

$$\delta_{\max} = \arctan \left[\frac{v^2}{m_1^2 (c^2 - 1)} \right]. \quad (18)$$

Fig. 1 shows the resulting bounds for the mass-splitting parameter c as a function of the mass, for two different, allowed values of the mixing angle. For $s_\delta \rightarrow 1(0)$, the upper bound becomes tighter (relaxed). Fig. 2 shows the resulting upper bound on s_δ as a function of the mass, for two given values of the mass-splitting parameter c . An increased (reduced) value of c implies a tighter (relaxed) upper bound on s_δ for a given mass. Note that the

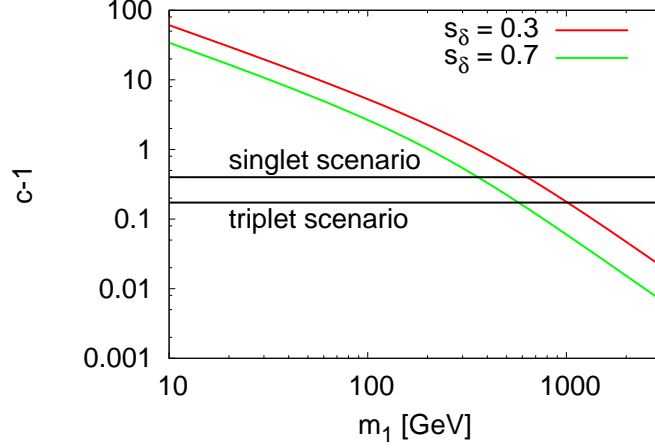


FIG. 1. The perturbative upper limit on the mass-splitting parameter c for two different values of the singlet-triplet mixing angle δ . The lines are upper exclusion contour lines.

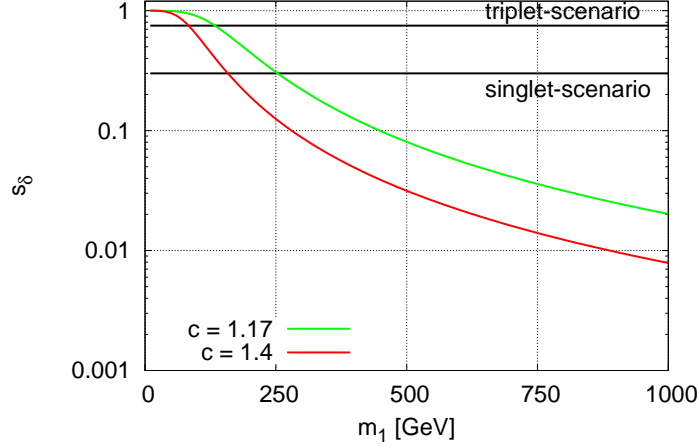


FIG. 2. The perturbative upper limit on the singlet-triplet mixing angle δ for two different values of the mass-splitting parameter c . The lines are upper exclusion contour lines.

black lines represent the separation of the singlet and the triplet scenario as defined below. In Fig. 2, the excluded range of the mixing angle is within the black lines.

Considering Z boson decays into a pair of charged S^{\pm} , the associated partial decay width is $\mathcal{O}(1 \text{ GeV})$, for m_c not close to or above the decay threshold. The experimental limit is $\Gamma_{Z \rightarrow x\bar{x}} \leq 4.2 \text{ MeV}$ [19], with x being a non SM particle. This limit is a lower bound on the triplet mass:

$$m_c > \frac{m_Z}{2}. \quad (19)$$

III. DARK MATTER PROPERTIES

The dark matter relic density can be inferred from WMAP [20] and Planck [21] data. An analysis which combines the results from both experiments yields the value

$$\Omega_{DM}h^2 = 0.1199 \pm 0.0027. \quad (20)$$

We shall use this value as constraint on the model parameters in the following, and quote it with *abundance* constraint.

The lightest Z_2 odd field S_1 is the dark matter candidate of the singlet-triplet Z_2 model. It couples to the Higgs boson and the gauge fields. For a very small value of δ the Higgs coupling is dominant in the annihilation cross section of the S_1 , so that the model is expected to behave similar to the pure scalar singlet model [3–8]. For $\delta \rightarrow \pi/2$, the gauge couplings become dominant in the annihilation cross section of the S_1 , making the model similar to the pure triplet model [9–11].

Considering the heavier S_i , S_j , their coannihilations are suppressed by a Boltzmann factor

$$\ln B = -X_f \left(\frac{m_i + m_j - 2m_1}{m_1} \right), \quad (21)$$

with the masses $m_i, m_j \in (m_2, m_c)$ and X_f the freeze-out temperature of the S_1 . The numerical tool MicrOMEGAs considers these processes up to $\ln B = -13.8$. For the coannihilations of the S^\pm , with $m_i = m_j = c m_1$, this yields the function for the mass-splitting parameter c :

$$f_c(X_f) = 1 + \frac{6.9}{X_f}. \quad (22)$$

This function serves as a benchmark, whether S^\pm coannihilations are being included in the computation of the abundance. Since typical WIMP freeze-out temperatures vary between 20 and 40, for values of the mass-splitting parameter given by $c \geq f_c(20) = 1.345$, coannihilations are not considered by micrOMEGAs. Conversely, for $c \leq f_c(40) = 1.1725$ the coannihilations of the other particles are included into the computation of the relic abundance.

A. Singlet Scenario

We define the *singlet scenario*, so that the S_1 abundance is dependent on the mass m_1 and the Higgs coupling ω_{11} , comparable to the pure scalar singlet model as in Refs. [3, 4, 7],

in the following way:

$$s_\delta \leq 0.3 \quad \text{and} \quad c \geq 1.4. \quad (23)$$

The annihilation cross section is dominated by Higgs exchange, the strength of which is controlled by ω_{11} . The coannihilations of the S^\pm fields are negligible according to eq. (22). Notice that the choice for the limiting values for s_δ and c is somewhat arbitrary. In this scenario, the abundance constraint can be matched by tuning the parameters m_1 , ω_{11} , and, to a lesser extent, δ .

The mass range for m_1 for a given δ is constrained by the perturbativity of the couplings:

$$m_1 < \frac{246 \text{ GeV}}{\sqrt{t_\delta(c^2 - 1)}}, \quad (24)$$

which for $s_\delta = 0$ and $c \geq 1.4$ recovers the limits on the mass range from the pure singlet model, which comes from the constraint $|\omega_{11}| \leq 1$, and eq. (20). This is illustrated by the red area in Fig. 3, which represents allowed values for the abundance. The mass is limited from above by $m_1 \leq 3.4 \text{ TeV}$. The green curve in the figure represents the case of $s_\delta = 0.3$ and $c = 1.4$. It diverges from the red area at $m_1 = 457 \text{ GeV}$, in agreement with the formal upper bound on m_1 from eq. (24). This divergence is due to ω_{12} becoming larger than one, growing proportional to m_1^2 . This increases σ_A through contributions from coannihilations of the form $S_1 S_2 \rightarrow h \rightarrow f \bar{f}$, suppressing the abundance. An increase of c does increase the Boltzmann suppression, but at the same time it also increases the coupling ω_{12} .

Considering the mass spectrum in the singlet scenario, the parameter $c \geq 1.4$ determines the mass splitting between the S_1 and the S^\pm fields. The relative mass splitting between the S^\pm and the S_2 is given by eq. (11). For $s_\delta = 0$ it is $c_2 = c$, and the two heavier fields are mass degenerate, apart from the radiative corrections to the S^\pm . The maximum value for c_2 is given with $c_2^{\text{max}} = 1.05$ for large c and $s_\delta = 0.3$.

Subsequently, the S_2, S^\pm form a set of fields that is similar to the three fields in the pure triplet model. We point out two differences. First, the S_2 tends to be heavier than the S^\pm . Second, the relative mass difference between S_2 and S^\pm does not converge to zero for large masses.

In the singlet scenario, the coannihilations and the perturbative constraints on the parameter c are negligible for $m_1 \sim m_H/2$. Therefore, the most recent constraints from the direct detection experiment LUX [22] affect the mass range in the same manner as in the pure singlet model. This places the lower bound of 53 GeV on m_1 and also excludes the

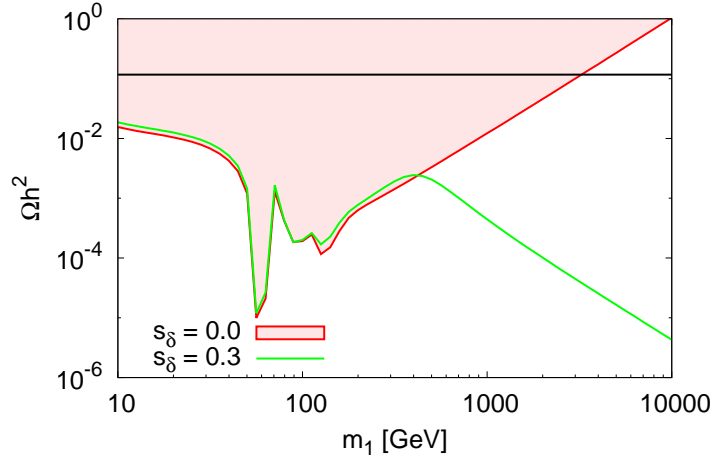


FIG. 3. Abundance of the singlet scenario as a function of the mass m_1 . The red area represents values which are allowed by the constraints on the parameter space. For the green curve, $s_\delta = 0.3$ has been used. For $m_1 = 457$ GeV the two lines diverge due to $\kappa > 1$, see eq. (24).

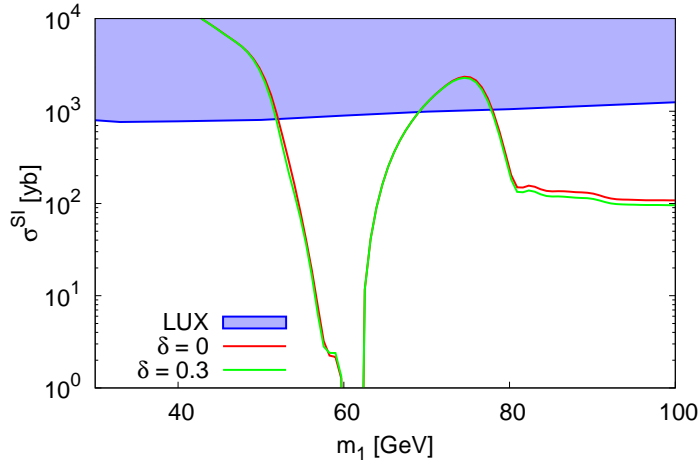


FIG. 4. Direct detection constraints on the mass parameter in the singlet scenario. The spin independent S_1 -nucleon cross section is displayed in yoctobarn. The blue area represents the most recent exclusion limits from the LUX experiment [22], the red line represents the abundance constraint from WMAP and Planck data on the coupling of the S_1 to the Higgs boson.

mass range $66 \text{ GeV} \leq m_1 \leq 78 \text{ GeV}$, as shown in Fig. 4. This range is not visibly affected by the variation of s_δ between zero and 0.3, so that the mass range for the S_1 is given by $78 \text{ GeV} \leq m_1 \leq 3.4 \text{ TeV}$, except for the narrow range around the Higgs resonance.

We note at this point that here and in the following, we use the value for the strangeness

of the nucleon as reported in Ref. [23].

B. Triplet Scenario

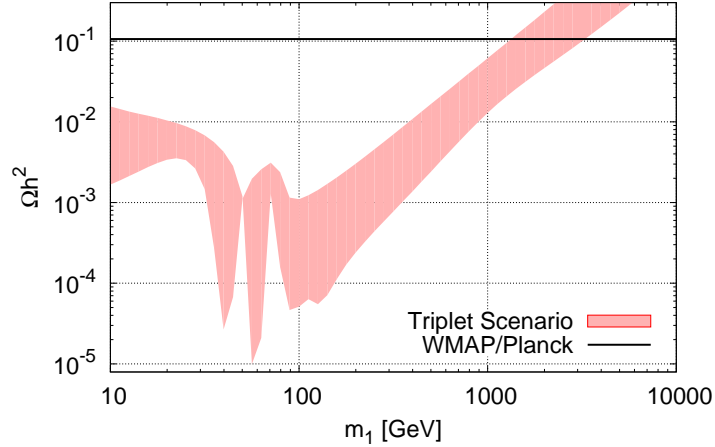


FIG. 5. Abundance of the triplet scenario as a function of the mass m_1 . The red area represents values for the abundance, resulting from a maximum variation of the coupling constants ω_{11}, ω_{22} , the singlet-triplet mixing angle s_δ and the mass-splitting parameter c . The black line represents the abundance constraint from WMAP [20] and Planck [21], its uncertainty is too small to show in this plot.

We define the *triplet scenario*, so that the abundance is qualitatively close to that of the pure triplet model as in Refs. [9–11], by the following constraints:

$$s_\delta \geq 0.75 \quad \text{and} \quad c < 1.17. \quad (25)$$

Because of the small value for c , the coannihilations of the S^\pm fields are contributing to σ_A , resulting in an increased sensitivity of the abundance on the couplings $\omega_{22}, \omega_{12}, \omega_\Psi$, compared to the singlet scenario. The large value of s_δ yields strong gauge couplings of the S_1 field, which in turn reduces the sensitivity to ω_{11} .

The mass-splitting parameter c is very powerful in controlling the contributions from the S^\pm, S_2 to the abundance, and their coannihilation strength. For c close to one, the Boltzmann suppression of the S^\pm, S_2 abundances becomes negligible, which contributes to, and thus increases the, S_1 abundance. For a suitable choice of c, s_δ , the coannihilations of

the S_2 still contribute to σ_A , while its abundance is still suppressed. In this extreme case, Ω can take smaller values compared to the abundance in the triplet model for the same mass. On the other hand, if $c \simeq 1$, the abundance can be larger than in the triplet model.

This makes the abundance being mainly sensitive to the variation of m_1 and c , and only minorly to a tuning of the Higgs couplings. Fig. 5 shows how the variation of the parameters $\omega_{11}, \omega_{22}, s_\delta, c$ affect the abundance. The upper boundary of the red area is given for $s_\delta = 0.75$ and $c, c_2 \simeq 1$. The lower boundary is given for $s_\delta = 1 - \varepsilon$, with $\varepsilon \rightarrow 0$ for numerical stability, and $c \sim c_{\text{max}}$. The variation of the model parameters allows for the S_1 mass in the range of

$$1.33 \text{ TeV} \leq m_1 \leq 6.65 \text{ TeV} , \quad (26)$$

to match the abundance constraint. It is possible to constrain the mass range in eq. (26) with gamma ray data from the HESS collaboration [24]. Adopting an NFW profile, this translates into a limit on the mixing angle:

$$s_\delta < \left(\frac{\Omega_1}{\Omega_{\text{HESS}}} \right)^{\frac{1}{4}} . \quad (27)$$

For m_1 between ~ 2 and ~ 3 TeV, the Hess constraints limit the angle from above with $s_\delta < 0.75$ and therefore exclude the triplet scenario. We emphasize however, that this constraint is strongly dependent on the choice of the halo profile model [25, 26].

Concerning the mass splitting between the three fields, we first consider the effect of the constraints on the parameter c . The abundance constraint limits the mass splitting parameter to $c \leq 1.001$. The upper limit for m_1 is given by (26). We define the absolute value of the mass splitting between the three masses with

$$\Delta_{ij} = m_i - m_j . \quad (28)$$

The upper limits for the Δ_{ij} , with $i = 2, c$ and $j = c, 1$, are shown in Fig 6. The absolute values of the upper bounds for the three parameters grow as large as ~ 20 GeV for $m_1 \rightarrow 6.5$ TeV. The ranges for the mass splittings are given by:

$$0 \leq \Delta_{21} \leq 19.4 \text{ GeV} , \quad (29)$$

$$-0.168 \text{ GeV} \leq \Delta_{2c} \leq 16.6 \text{ GeV} , \quad (30)$$

$$0.168 \text{ GeV} \leq \Delta_{c1} \leq 2.8 \text{ GeV} , \quad (31)$$

which may have consequences for collider searches, as it opens up more decay channels.

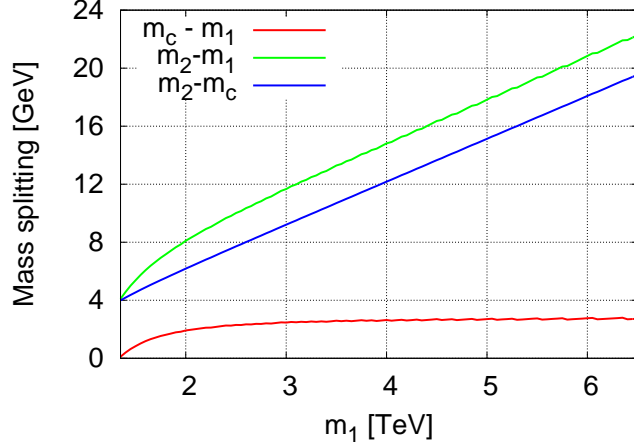


FIG. 6. The mass splittings Δ_{ij} for $i = 2, c$ and $j = c, 1$ between S_1, S_2, S^\pm in the triplet scenario. The lines represent upper limits on the absolute values of the three different mass splittings.

C. Intermediate Scenarios

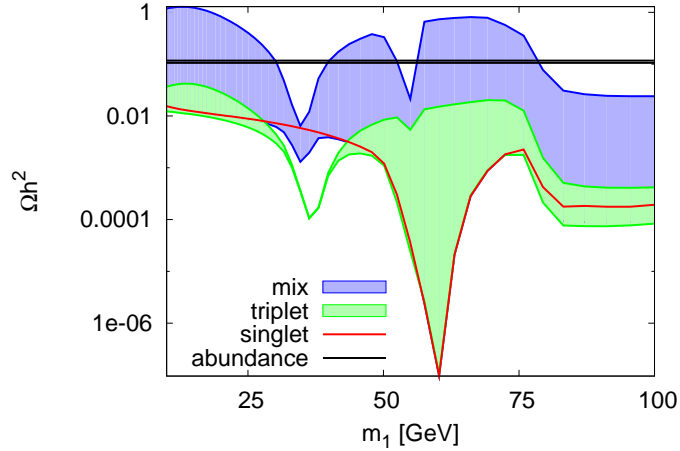


FIG. 7. The relic density as a function of mass m_1 for three different scenarios. The width of the blue and green area represents the variation of ω_{11}, ω_{22} between 0 and 1. For the singlet scenario $c = 1.4$ and $s_\delta = 0$ have been used, the intermediate scenario uses $c = 1.2$ and $0.35 \leq s_\delta \leq 0.75$, excluding the range leading to $|\kappa| > 1$. For the triplet scenario, $s_\delta = 0.9$ and $c = 1.1$ were used.

We define the *intermediate scenario* by the range that remains uncovered by the singlet and triplet scenario:

$$0.3 < s_\delta < 0.75 \quad \text{and} \quad 1.17 < c < 1.4. \quad (32)$$

The intermediate scenario is displayed in Fig. 7, together with the singlet and the triplet scenario. We choose the mass range between 10 and 100 GeV to illustrate the effects of coannihilations and the gauge interactions of the S_1 . The blue and green areas represent the intermediate and triplet scenario, respectively. The width of each area is given by the variation of the Higgs couplings ω_{11}, ω_{22} , between 0 and 1. The red line represents the lower contour line for the singlet scenario. The black line denotes the abundance constraint from eq. (20), which implies that the triplet scenario is excluded in this low mass range, while the intermediate scenario is able to match the constraint for a tightly constrained mass range.

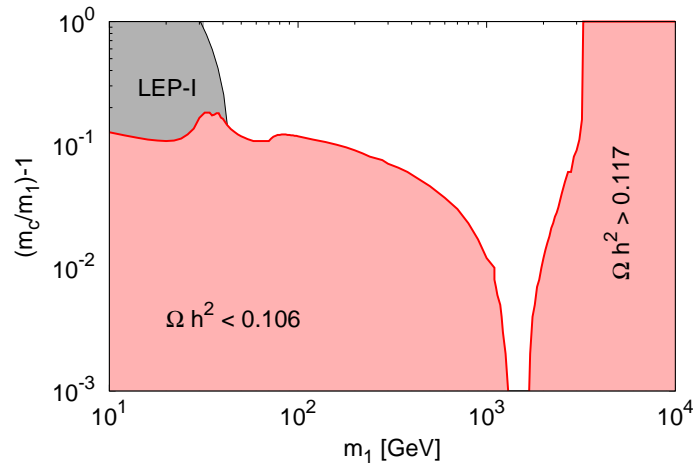


FIG. 8. Allowed range for the mass-splitting parameter c as a function of the mass m_1 . The red area represents parameter sets being excluded by WMAP and Planck data, the dark gray area represents the partial Z boson decay width into S^\pm violating LEP-I limits [19].

The Z and W^\pm boson resonances are Boltzmann suppressed in the singlet scenario, their magnitude is proportional to s_δ . The resonance of the weak gauge bosons is shifted to smaller values of m_1 due to the center-of-mass energy of the associated process, $S_1 S^\pm \rightarrow W^\pm \rightarrow f^0 f^\pm$, with f^0, f^\pm being neutral and charged Standard Model fields, being the sum of the dark matter masses.

With $s_\delta = 0$ and $\omega_{11} \sim 0$, the abundance is given as a function of the mass splitting. For each mass there exists a value $c > 1$, so that the coannihilations alone satisfy the abundance constraint. Fig. 8 illustrates this critical value for c . For a parameter set m_1, c above this critical line, a choice of the Higgs couplings and s_δ exists, so that the abundance constraint can be met. The red area is excluded by the abundance constraint in eq. (20). For the S_1

mass in the range $1.33 \text{ TeV} \leq m_1 \leq 1.68 \text{ TeV}$, the coannihilations have the appropriate annihilation efficiency to match the abundance constraint, so that $c = 1$ is allowed.

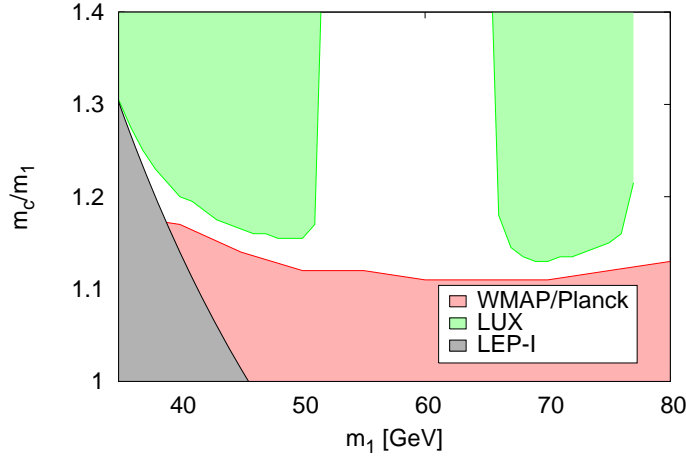


FIG. 9. Parameter space in the relaxed singlet model. The red area represents a dark matter relic abundance being too small compared to the value reported by WMAP/Planck. The green area represents the combination of the abundance constraint from WMAP [20] and Planck [21] with the direct search constraints from LUX [22]. The gray area denotes the decays of the Z boson into S^\pm violating LEP-I exclusion limits [19].

We define the *relaxed singlet scenario* with the following constraints:

$$s_\delta < 0.3 \quad \text{and} \quad c < c_{\text{max}}. \quad (33)$$

This definition includes the coannihilations of the S^\pm . In this way small values of ω_{11} are not necessarily excluded through the abundance constraint. We say that the abundance constraint on the Higgs coupling is relaxed.

For c close to border of the red area in Fig. 8, the abundance constraint on ω_{11} can become arbitrarily small. This allows for a spin-independent S_1 nucleon scattering cross section, sufficiently small not to violate the direct search exclusion limits from the LUX experiment for $m_1 \leq 53 \text{ GeV}$ and also for $66 \text{ GeV} \leq m_1 \leq 78 \text{ GeV}$.

The uncolored area in Fig. 9, framed by the exclusion limits from LUX, WMAP, Planck and LEP-I, can accommodate all constraints simultaneously. The LEP-I limits come from upper bounds on the Z boson decay width as in eq. (19). The green area represents the value of σ^{SI} , as given by the abundance constraint on ω_{11} , being excluded by the exclusion limits

from the LUX experiment. The red area denotes coannihilations suppressing the abundance below the abundance constraint in eq. (20). Thus, the lower bound on the mass m_1 is given by ~ 35 GeV in this scenario.

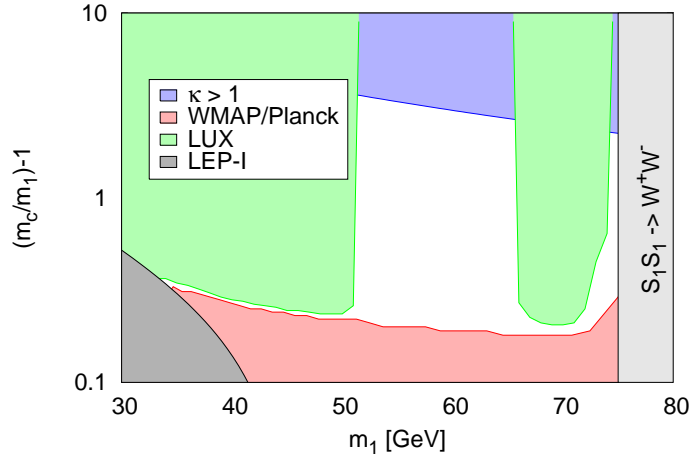


FIG. 10. Parameter space of the relaxed triplet scenario. The red area represents the WMAP/Planck exclusion limits, the green area denotes the combination of the abundance constraint and the direct search exclusion limits on the spin-independent S_1 -nucleon scattering cross section (σ^{SI}) from LUX [22]. The blue area denotes the upper bound from perturbativity and the gray area the suppression of the abundance by the coannihilations of the S^\pm , and the gray area the exclusion limits from LEP-I [19].

We define the *relaxed triplet scenario* by constraining

$$s_\delta > 0.75 \quad \text{and} \quad 1.4 < c < c_{\text{max}}. \quad (34)$$

This suppresses coannihilations and increases the sensitivity of the abundance to ω_{11} . We notice, that the condition in eq. (24) limits m_1 from above with 238 GeV.

Fig. 10 shows the areas of parameter space for which the abundance constraint in eq. (20) can be met by a variation of ω_{11} . For values of c and m_1 as defined by the red area, the coannihilations are too efficient. The blue area denotes the perturbative constraint. For masses $m_1 \sim M_W$, the W boson production threshold is reached. Due to virtual W production, this threshold is given with 75 GeV. For m_1 at the threshold and beyond, the four-point interaction between the S_1 and the W bosons dominates the total annihilation

cross section efficiency, which is too large to match the abundance constraint for allowed masses. Thus the upper limit of m_1 in this scenario is given by 75 GeV.

WMAP/Planck data constrains ω_{11} for m_1, c in the allowed range, which fixes the value of σ^{SI} . The green area in Fig. 10 shows the LUX exclusion limits on the parameter space. Altogether, the relaxed triplet scenario confines the mass m_1 to the range $51 \text{ GeV} \leq m_1 \leq 75 \text{ GeV}$.

The absolute values of the mass splittings Δ_{ij} in this scenario can become very large. In particular $c = 3.2$ is possible, and with $m_2 = c/c_\delta$, c_2 is constrained by perturbativity. This leads to a decay spectrum with large mass splittings for $m_1 \simeq 51 \text{ GeV}$ and $s_\delta = 0.75$

$$51.1 \text{ GeV} \leq \Delta_{21} \leq 366 \text{ GeV}, \quad (35)$$

$$10.2 \text{ GeV} \leq \Delta_{c1} \leq 115 \text{ GeV}, \quad (36)$$

$$40.9 \text{ GeV} \leq \Delta_{2c} \leq 251 \text{ GeV}. \quad (37)$$

IV. CONCLUSIONS

In this paper we introduced the singlet-triplet Z_2 model. In this model an additional singlet and $SU(2)_L$ triplet field reside in the odd representation of a global Z_2 symmetry. Spontaneous symmetry breaking induces mass mixing among the neutral Z_2 odd fields, which renders the lightest one a suitable candidate for cold dark matter.

We investigated the constraints from WMAP and Planck data, the direct search experiment LUX, LEP-I and perturbativity on the model parameter space. The latter can be separated in three distinct scenarios. The first of these is the singlet scenario. It is comparable to the pure scalar singlet model, where the coupling between the Higgs boson and the dark matter and the dark matter mass parameter are the most relevant parameters. In this scenario the ranges of $51 \text{ GeV} \leq m_1 \leq 66 \text{ GeV}$ and $78 \text{ GeV} \leq m_1 \leq 3.4 \text{ TeV}$ are allowed for the mass of the dark matter candidate. The heavier neutral and the charged Z_2 odd particles are nearly mass degenerate, which results in detector signatures as difficult to detect at a collider as in the case of the pure triplet model [10]. The mass splitting between S^\pm and S_1 , however, can be $\mathcal{O}(100 \text{ GeV})$ for $m_1 \approx 1 \text{ TeV}$, which allows for decays of the form $S^\pm \rightarrow S_1 f^\pm$, with f^\pm being any Standard Model field with an even charge.

The second scenario is the triplet scenario, where coannihilations are relevant and the total

annihilation cross section is dominated by the gauge couplings. This scenario is very close to the pure triplet model. The extra parameters extend the range for the dark matter mass to $1.33 \text{ TeV} \leq m_1 \leq 6.65 \text{ TeV}$. Gamma ray data from the HESS collaboration can constrain this mass range further, however in a way that is highly dependent on the model for the halo. The mass splitting between the neutral and charged components are bounded from above with 2.8 GeV for the lightest and charged fields, and to $\mathcal{O}(10 \text{ GeV})$ for the other two combinations, respectively.

The third scenario is an intermediate one, which includes two interesting sub scenarios: The relaxed singlet scenario demands a small mixing angle, but allows for the inclusion of coannihilations. This relaxes the abundance constraint on the S_1 -Higgs coupling, which allows for a reduction of the lower bound on m_1 to 35 GeV. In the relaxed triplet scenario, the neutral triplet component constitutes the dominant part of the dark matter candidate, and coannihilations are suppressed. This leads to a range for the dark matter mass between 51 and 75 GeV.

In the relaxed scenarios, some of the mass-splittings between the S_1, S^\pm, S_2 can become larger than M_W . This has consequences for collider searches, because a mass splitting above the M_W threshold allows for the decays $S_2 \rightarrow S^\pm W^\mp$ and $S^\pm \rightarrow S_1 W^\pm$. These decays should lead to more detectable signatures at the LHC compared to the signals from the decay into rather soft SM particles in the triplet scenario.

ACKNOWLEDGEMENTS

This work was supported by the Deutsche Forschungsgemeinschaft (DFG) through the Graduate School GRK 1102 "Physik an Hadron-Beschleunigern" and by the Bundesministerium für Bildung und Forschung within the Förder-schwerpunkt *Elementary Particle Physics*. We thank Drs. Lorenzo Basso and Andrea Banfi for a careful reading of the manuscript, Prof. Dan Akerib and Dr. Blair Edwards from Yale for helpful assistance with the LUX data. Further we acknowledge the use of the Legacy Archive for Microwave Background Data Analysis (LAMBDA). Support for LAMBDA is provided by the NASA Office

of Space Science.

- [1] F. Zwicky, “Spectral displacement of extra galactic nebulae,” *Helv.Phys.Acta*, vol. 6, pp. 110–127, 1933.
- [2] V. C. Rubin and J. Ford, W. Kent, “Rotation of the Andromeda Nebula from a Spectroscopic Survey of Emission Regions,” *Astrophys.J.*, vol. 159, pp. 379–403, 1970.
- [3] V. Silveira and A. Zee, “Scalar Phantoms,” *Phys.Lett.*, vol. B161, p. 136, 1985.
- [4] J. McDonald, “Gauge singlet scalars as cold dark matter,” *Phys.Rev.*, vol. D50, pp. 3637–3649, 1994.
- [5] T. Binoth and J. van der Bij, “Higgs signals modified by singlet scalars,” 1994.
- [6] T. Binoth and J. van der Bij, “Influence of strongly coupled, hidden scalars on Higgs signals,” *Z.Phys.*, vol. C75, pp. 17–25, 1997.
- [7] C. Burgess, M. Pospelov, and T. ter Veldhuis, “The Minimal model of nonbaryonic dark matter: A Singlet scalar,” *Nucl.Phys.*, vol. B619, pp. 709–728, 2001.
- [8] C. Boehm and P. Fayet, “Scalar dark matter candidates,” *Nucl.Phys.*, vol. B683, pp. 219–263, 2004.
- [9] R. Barbieri, L. J. Hall, and V. S. Rychkov, “Improved naturalness with a heavy Higgs: An Alternative road to LHC physics,” *Phys.Rev.*, vol. D74, p. 015007, 2006.
- [10] P. Fileviez Perez, H. H. Patel, M. Ramsey-Musolf, and K. Wang, “Triplet Scalars and Dark Matter at the LHC,” *Phys.Rev.*, vol. D79, p. 055024, 2009.
- [11] M. Cirelli, N. Fornengo, and A. Strumia, “Minimal dark matter,” *Nucl.Phys.*, vol. B753, pp. 178–194, 2006.
- [12] M. Kadastik, K. Kannike, and M. Raidal, “Matter parity as the origin of scalar Dark Matter,” *Phys.Rev.*, vol. D81, p. 015002, 2010.
- [13] J. van der Bij, “A Cosmotopological relation for a unified field theory,” *Phys.Rev.*, vol. D76, p. 121702, 2007.
- [14] J. van der Bij, “Gravitational anomaly and fundamental forces,” *Gen. Relativ. Gravit.*, 2010.
- [15] E. Aprile *et al.*, “Dark Matter Results from 100 Live Days of XENON100 Data,” *Phys. Rev. Lett.*, vol. 107, p. 131302, 2011.

- [16] O. Fischer and J. van der Bij, “Multi-singlet and singlet-triplet scalar dark matter,” *Mod.Phys.Lett.*, vol. A26, pp. 2039–2049, 2011.
- [17] G. Belanger, F. Boudjema, A. Pukhov, and A. Semenov, “Micromegas,” *Comput.Phys.Commun.*, vol. 149, pp. 103–120, 2002.
- [18] G. Belanger, F. Boudjema, A. Pukhov, and A. Semenov, “micrOMEGAs: Version 1.3,” *Comput.Phys.Commun.*, vol. 174, pp. 577–604, 2006.
- [19] J. Beringer *et al.*, “Review of Particle Physics (RPP),” *Phys.Rev.*, vol. D86, p. 010001, 2012.
- [20] G. Hinshaw *et al.*, “Nine-Year Wilkinson Microwave Anisotropy Probe (WMAP) Observations: Cosmological Parameter Results,” *Astrophys.J.Suppl.*, vol. 208, p. 19, 2013.
- [21] P. Ade *et al.*, “Planck 2013 results. XVI. Cosmological parameters,” 2013.
- [22] D. Akerib *et al.*, “First results from the LUX dark matter experiment at the Sanford Underground Research Facility,” 2013.
- [23] J. Alarcon, L. Geng, J. Martin Camalich, and J. Oller, “On the strangeness content of the nucleon,” 2012.
- [24] A. Abramowski *et al.*, “Search for a Dark Matter annihilation signal from the Galactic Center halo with H.E.S.S.,” *Phys.Rev.Lett.*, vol. 106, p. 161301, 2011.
- [25] J. Fan and M. Reece, “In Wino Veritas? Indirect Searches Shed Light on Neutralino Dark Matter,” *JHEP*, vol. 1310, p. 124, 2013.
- [26] T. Cohen, M. Lisanti, A. Pierce, and T. R. Slatyer, “Wino Dark Matter Under Siege,” *JCAP*, vol. 1310, p. 061, 2013.